Imaging beneath gas clouds using 3D prestack Kirchhoff time migration of PS-converted waves—A case study from the North Sea

Hengchang Dai and Xiang-Yang Li, British Geological Survey, Edinburgh, UK
Paul Conway, Kerr-McGee North Sea (UK), Aberdeen, UK

We present a practical approach to imaging structures beneath gas clouds using PS-converted waves. In this approach, we developed methods to build the migration velocity model and to perform 3D prestack Kirchhoff time migration on a PC cluster and improved the processing flow for PS-converted waves. The technique was successfully applied to a 3D/4-C marine data set acquired in August 2001 and made available to us by Kerr-McGee North Sea (UK).

This was a North Sea survey with a nominal receiver area of 10.8 km^2. Two swath data sets were acquired. Each swath data set had an inline geometry using two receiver cables and 22 shot lines. The survey was centered on a domed structure which is obscured by a gas chimney. Faulting is thought to be present beneath the summit of the dome. Because the P-waves are attenuated by gas clouds, the P-wave image of the structure beneath the gas chimney is dimmed, but PS-converted waves can image that structure. In this study, we processed the PS-converted wave data of the 3D/4-C data set from one swath. The objective of the processing was to define the top of the structure at the reservoir target level (3.0 s PP time and 5.5 s PS time). We demonstrated how the PS-converted wave processing was able to clarify structural details.

3D prestack Kirchhoff time migration (PKTM) and an appropriate migration velocity model play a crucial role in imaging structures beneath gas clouds using PS-converted waves. Firstly, we present the principle of 3D PKTM and its implications for a PC cluster. Then we demonstrate how to build the migration velocity model. After that we show the results of 2D processing of P- and PS-converted waves for 2D lines at the location of receiver cables, and the results of 3D processing of PS-converted waves for one swath data set. Finally, we present the interpretation results based on the 3D migrated images and our conclusions.

Principles of 3D PKTM. 3D PKTM can produce an image at any desired location in a 3D space. Figure 1 shows the relationship among the scatterpoints (image points), shots, and receivers in 3D PKTM. The energy from a trace related to a shot and a receiver must be distributed to all possible scatterpoints in a surface according to the relevant traveltime. In other words, the energy from all shots and receivers is summed at each location to construct an image of the scatterpoints. This is usually implemented as a weighted summation based on the raypaths.

In 3D PKTM, the traveltime of a PS-converted wave (t_{ps}) for anisotropic media is calculated using the double-square-root (DSR) equation derived by Li et al. (2001):

$$t_{PS}=\sqrt{t_{P0}^2+\frac{x_P^2}{v_P^2}-\frac{2\eta_{\text{eff}}x_P^4}{v_P^2[t_{P0}^2v_P^2+(1+2\eta_{\text{eff}})x_P^2]}}+\sqrt{t_{S0}^2+\frac{x_S^2}{v_S^2}+\frac{2\xi_{\text{eff}}x_S^4}{v_S^2[t_{S0}^2v_S^2+x_S^2]}} \quad (1)$$

where x_p is the horizontal distance from the source to the scatterpoint; x_s is the horizontal distance from the scatterpoint to the receiver; t_{p0} is the vertical traveltime for the P-wave; t_{s0} is the vertical traveltime for the S-wave; V_P is the velocity for the P-wave, and V_S is the velocity for the S-wave.

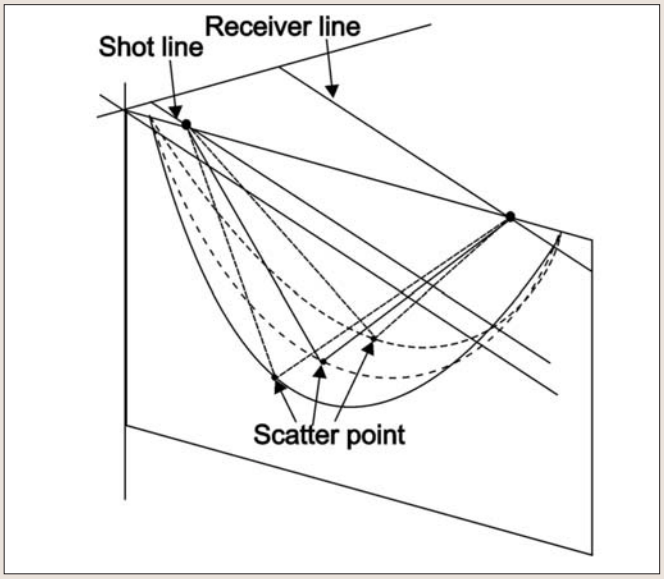

Figure 1. *The relationship between shots, receivers, and scatterpoints in 3D PKTM. For a given traveltime and raypath, the scatterpoints are on a surface in 3D space.*

η_{eff} and ξ_{eff} are anisotropy parameters for the P- and S-waves, respectively. However, the offset between the source and receiver does not equal $x_p + x_s$ when the shot line and receiver line are not collinear.

For PS-converted waves, it is difficult to obtain V_P and V_S from field data directly because only t_{ps} can be measured. It is not possible to separate t_{ps} into t_p and t_s. To overcome this difficulty, other parameters constructed from the above parameters can be used. One set of the combined parameters consists of the PS-converted wave velocity (V_{PS}), the effective velocity ratio (γ_{eff}), and vertical velocity ratio (γ_0). Li and Yuan (2003) recommend the parameter χ for describing the PS-converted wave anisotropy. The relationship between the two sets is defined as:

$$V_P^2=V_{PS}^2\frac{\gamma_{\text{eff}}(1+\gamma_0)}{1+\gamma_{\text{eff}}} \quad (2)$$

$$V_S^2=V_{PS}^2\frac{\gamma_{\text{eff}}(1+\gamma_0)}{(1+\gamma_{\text{eff}})\gamma_0} \quad (3)$$

$$\gamma_0=\frac{t_{S0}}{t_{P0}} \quad (4)$$

$$\gamma_{\text{eff}}=\frac{1}{\gamma_0}\left(\frac{V_P}{V_S}\right)^2 \quad (5)$$

$$\chi=\eta_{\text{eff}}\gamma_{\text{eff}}^2\gamma_0-\xi_{\text{eff}} \quad (6)$$

$$\xi_{\text{eff}}=\eta_{\text{eff}}\gamma_{\text{eff}}^2 \quad (7)$$

Equation 7 is strictly true only for a single layer. However, we find that it can also be used in multilayer media without losing accuracy. V_{PS}, γ_{eff}, and χ can be estimated from PS-converted waves alone using a data-driven approach, and

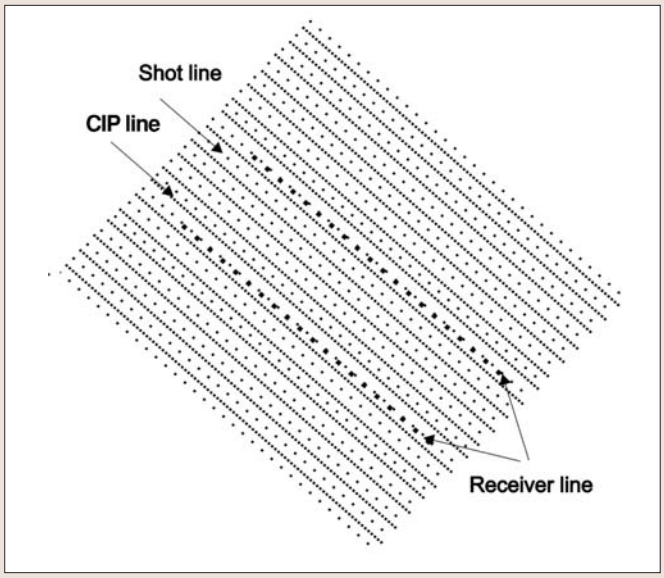

Figure 2. *The geometry of the shot lines, receiver lines, and CIP lines in 3D PKTM. The data from one shot line and one receiver line are migrated to all CIP lines. The final image at a CIP line is the summation of all subimages obtained from all shot and receiver lines.*

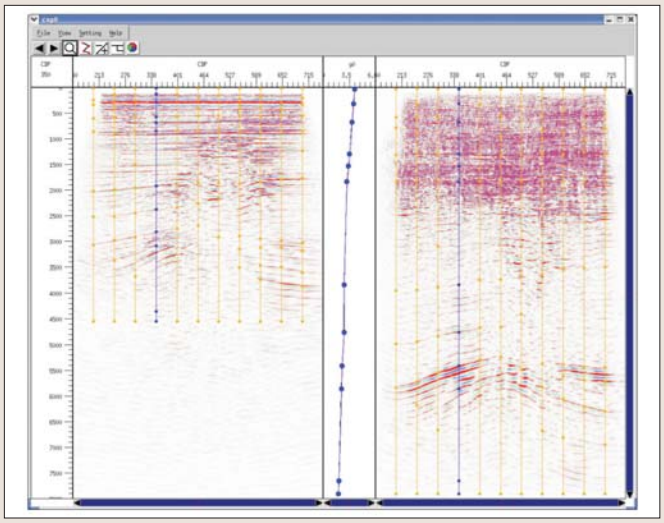

Figure 3. *Screen snapshot of the GUI tool of CXTools used to estimate γ_0 by correlating events in the P-wave and PS-converted wave sections. The left panel is a part of the P-wave section, and the right panel is the corresponding part of the PS-converted wave section. The middle panel shows estimated values of γ_0 at CDP 400.*

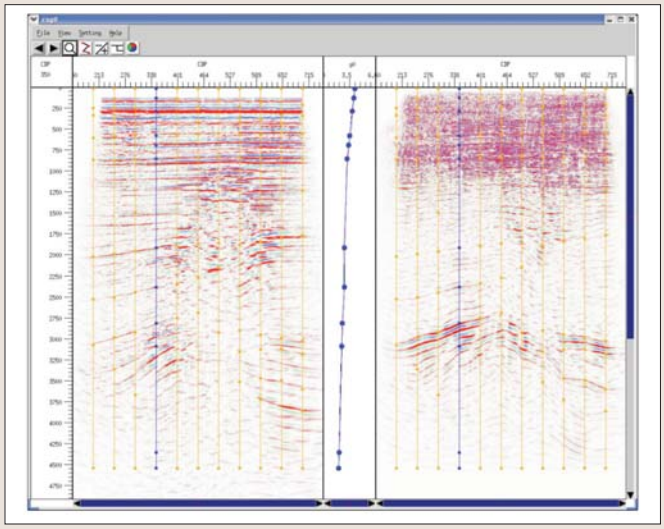

Figure 4. *Similar to Figure 3, with the PS-converted wave section displayed in PP time to allow comparison of P and PS sections.*

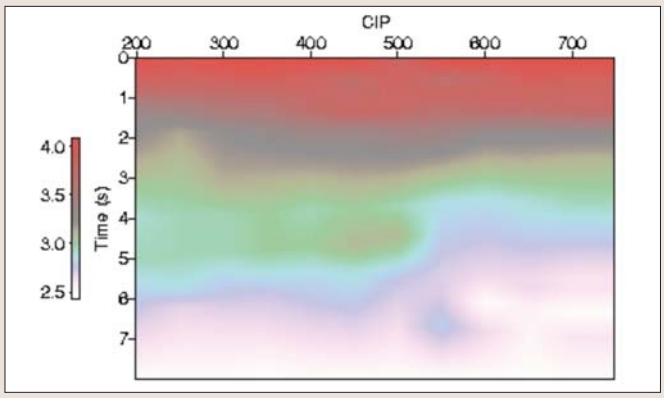

Figure 5. *Profile of γ_0 at the location of CIP line 050.*

γ_0 can be estimated from the correlation between events in the P-wave and PS-converted wave images. V_P and V_S are then calculated from V_{PS}, γ_{eff}, and γ_0; t_{p0} and t_{s0} are calculated from γ_0 and t_{c0}; and η_{eff} and ζ_{eff} are calculated from χ, γ_{eff}, and γ_0. The advantage of using V_{PS} and velocity ratios instead of V_P and V_S in PKTM processing is that the traveltime of the PS-converted wave is not sensitive to variations in the velocity ratios. The effect of velocity ratio error on the moveout is much less than the effect of V_{PS} error. In PS-converted wave data processing, the values of the velocity ratios obtained from stacking velocity analysis can be used in prestack time migration. Thus only the PS-converted-wave velocity needs to be estimated precisely.

In 3D PKTM, the locations of scatterpoints form a 3D image cube in the CIP (common image point) domain. The data from all shots and receivers contribute to every image point in this cube. However, a 3D/4-C data set often consists of tens of shot lines. The output cube is often very large and exceeds the capacity of normal computers. It is difficult to perform 3D PKTM for all shot lines in one run. To overcome this, we split the 3D image cube into CIP lines. Data from each pair of shot and receiver lines will contribute to any given CIP line (Figure 2) as a subimage of the CIP line. Then the 3D migrated image at the desired CIP line is the summation of all subimages obtained from all shot data for all receivers. This process can be written:

$$\text{image (cipline)} = \sum_{\text{shot}} \sum_{\text{receiver}} \text{subimage (cipline,shot,rec)} \quad (8)$$

where image(cipline) is the image at the location of one CIP line in the 3D cube and subimage (cipline, shot, rec) is the image at the location of the CIP line obtained from data related to a pair of shot and receiver lines. The task of processing one subimage using 3D PKTM is defined as the basic processing unit, which runs on a PC cluster to speed up the processing. This approach has several advantages. Because each basic processing unit produces only one subimage (cipline, shot, rec) from one pair of shot and receiver lines, this task can run at any time on any computer. The migrated subimage (cipline, shot, rec) is then stored on the disk for the final summation. Because the basic processing units are independent of each other, failure of one basic processing unit does not affect others. The cost of rerunning one basic processing unit is small. Therefore, the whole job can be conveniently scheduled, and the process is stable and robust.

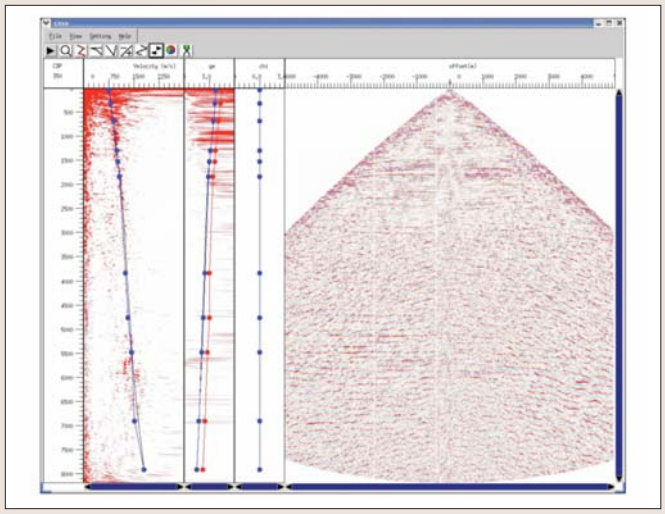

Figure 6. Screen snapshot of the GUI tool for an example at the location of CDP 350 of CIP line 050 from the data obtained from shot line 5002 and receiver line 5002. The far left panel shows the nonhyperbolic spectrum obtained from the ACP gather; the blue line indicates velocity values. The second panel shows γ_0 and γ_{eff}. The third panel shows χ. The right panel shows the ACP gather.

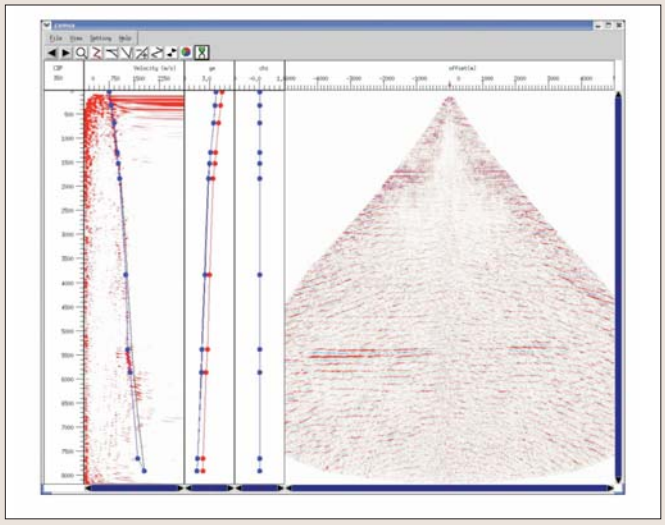

Figure 7. Screen snapshot of the GUI tool of an example at the location of CIP 350 of CIP line 050 from the data obtained from shot line 5002 and receiver line 5002. The left panel shows the hyperbolic spectrum obtained from the reverse NMO-CIP gather. The blue line indicates velocity values. The second panel shows γ_0 and γ_{eff}, and the third shows χ. The right panel shows the CIP gather. The target events at 5.35 s are flattened by updating the velocity model.

Migration velocity model estimation. An appropriate migration velocity model is critical for producing high-quality migrated images using PKTM. For PS-converted waves, a migration velocity model consists of V_{PS}, γ_{eff}, γ_0, and χ. Three steps are necessary to construct the velocity model for PKTM: (1) estimate γ_0 by correlating events in the P-wave and PS-converted wave stacked sections or migrated images; (2) estimate the stacking velocity model (V_{PS}, γ_{eff}, and χ) based on the nonhyperbolic anisotropic moveout analysis of the ACP (asymptotic-conversion-point) gathers of PS-converted waves; and (3) update the estimated stacking velocity model based on the hyperbolic moveout analysis of the inverted NMO-CIP gathers of PS-converted waves. Often V_{PS} is the only parameter that needs to be updated for PKTM. The stacking γ_{eff}, γ_0, and χ are set in the migration velocity model. Note that both the stacking velocity model and the migration velocity model are rms velocity models which are related to one CIP location. In 2D PKTM, all raypaths related to this CIP location have the same azimuth. However, in 3D PKTM, raypaths related to this CIP location have various azimuths. If azimuthal anisotropy is present, the migration velocity model should vary with azimuthal changes. If the variation is small, we may treat the migration velocity model as isotropic in azimuth.

The software used in this paper is CXTools as described in Dai (2003) and Dai and Li (2003).

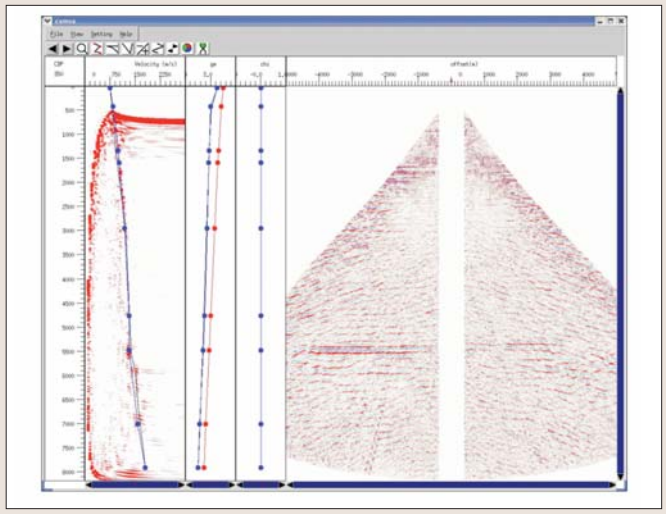

Figure 8. Screen snapshot of the GUI tool of another example at the location of CIP 350 of CIP line 050 from the data obtained from shot line 5018 and receiver line 5002. The target events at 5.35 s are also flattened by using the same velocity model.

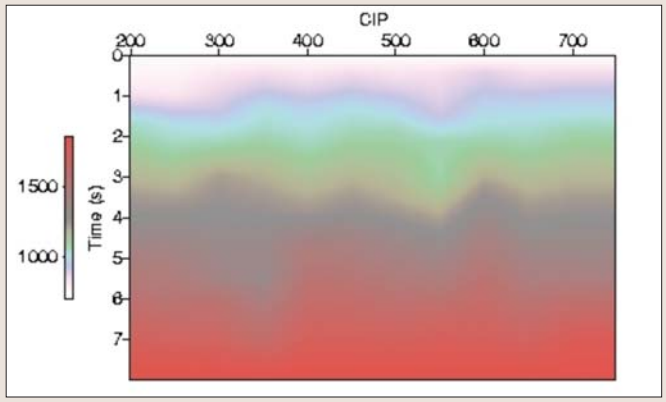

Figure 9. Profile of V_{PS} at the location of CIP line 050.

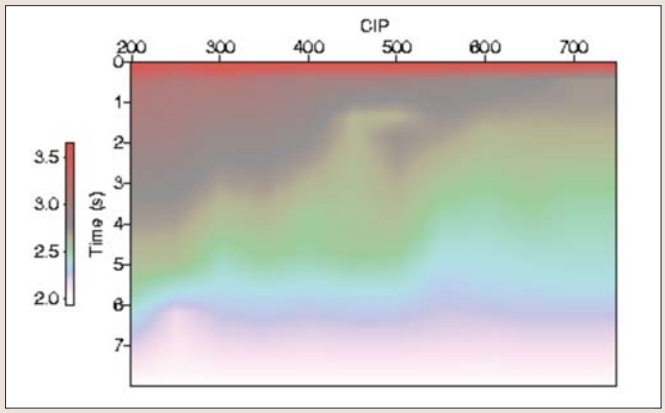

Figure 10. Profile of γ_{eff} at the location of CIP line 050.

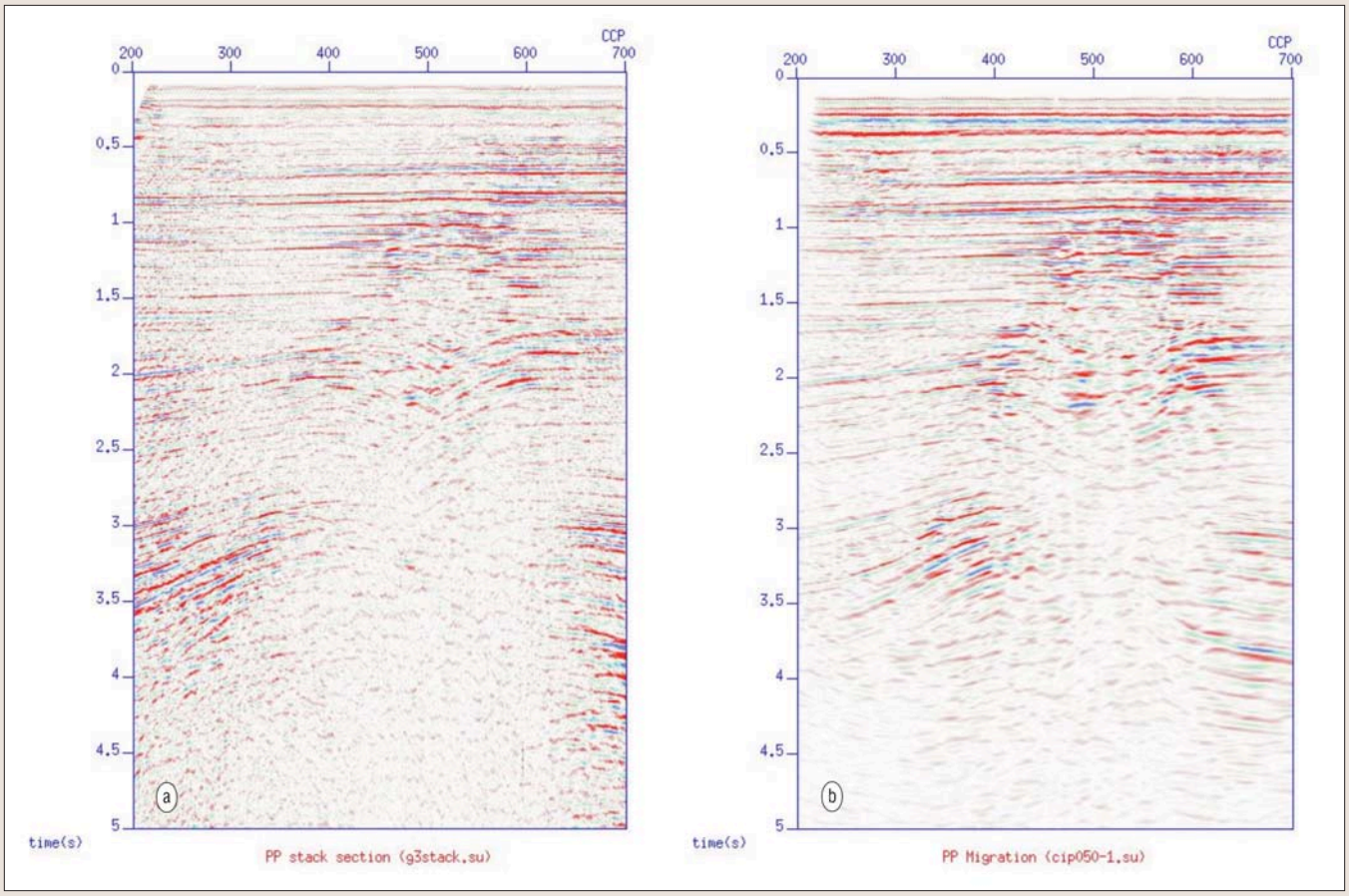

Figure 11. *Stacked section (a) and migrated image (b) of P-waves at receiver line 5002.*

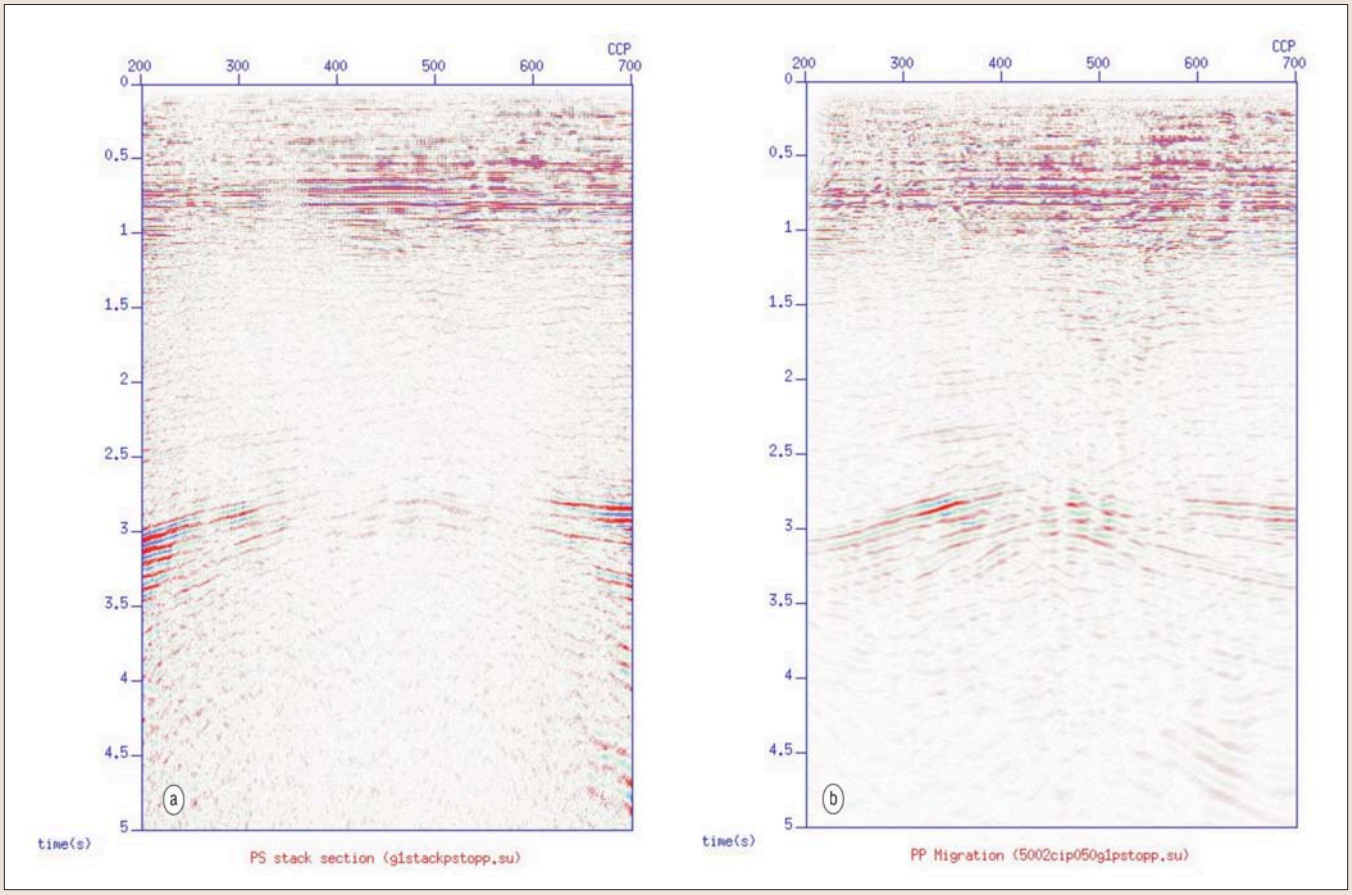

Figure 12. *Stacked section (a) and migrated image (b) of PS-converted waves displayed in PP time at receiver line 5002.*

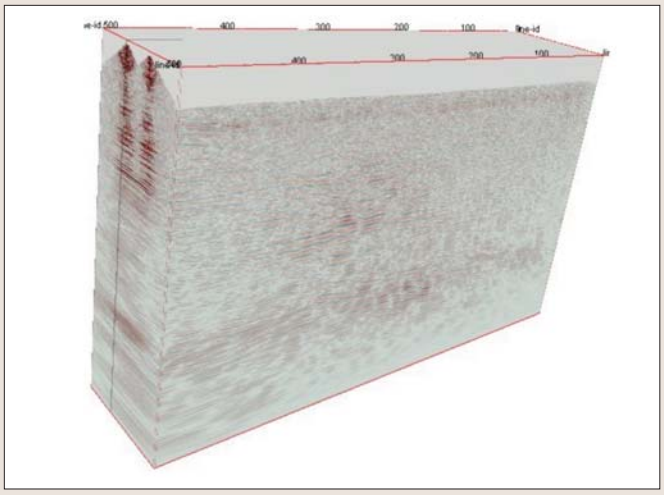

Figure 13. External display of the 3D cube of the migrated image.

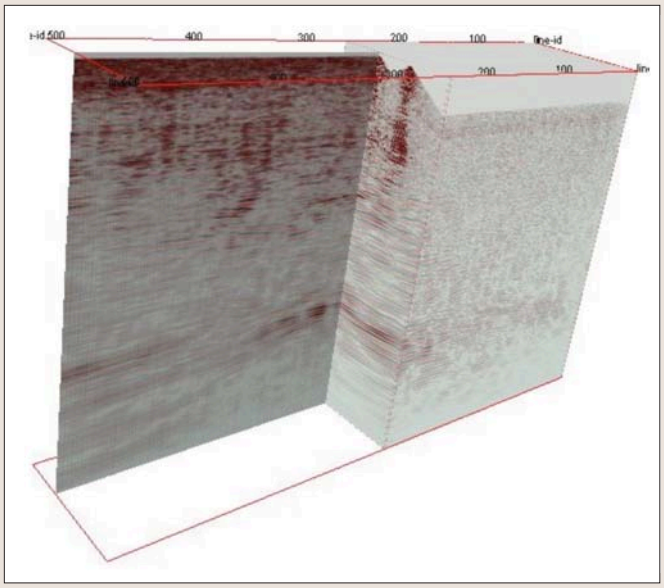

Figure 14. An internal display of the 3D cube of the migrated image.

Stacking velocity model estimation. Estimating the stacking velocity model is a typical 2D processing procedure and is only carried out on two 2D lines at the locations of CIP lines 050 (at receiver line 5002) and 070 (at receiver line 5018) where the source line overlaps on the receiver line. There are two steps: (1) estimating γ_0 by correlating events in the brute-stacked P-wave and PS-converted wave sections; (2) estimating V_{PS}, γ_{eff}, and χ from an ACP gather of PS-converted waves. Figure 3 shows examples of estimated γ_0 and the corresponding P-wave and PS-converted wave sections at the location of CIP line 050. The left panel in Figure 3 is the P-wave section, and the right panel is the PS-converted wave section. The middle panel gives the estimated values of γ_0 at CDP 400. Using the values of γ_0, we can convert the vertical traveltime of the PS-converted wave section to PP time. Figure 4 shows the converted-wave results. The events in the PS-converted wave section are well matched with the events in the P-wave section. Figure 5 shows the profile of γ_0 for this CIP line. Since the values of γ_0 are not sensitive in the time processing, we apply the values to all locations in this data set.

Once γ_0 is estimated, we estimate V_{PS}, γ_{eff}, and χ from ACP gathers of PS-converted waves. Figure 6 shows an example of the stacking velocity model and the corresponding ACP gather at the location of CDP 350 of receiver line 5002 (CIP line 050). The left panel shows the nonhyperbolic spectrum obtained from the ACP gather, and the blue line indicates the velocity values. The second panel shows the spectrum of γ_{eff} and the values of γ_0 and γ_{eff}; the third panel shows χ. The right panel shows the ACP gather. Note that we can flatten the events in the ACP gathers by setting $\chi = 0$ for both cases. This implies that either there is no VTI anisotropy or it is too small to be estimated.

Migration velocity model updating. Once the stacking velocity model is estimated, we use it as the initial migration velocity model in PKTM and update it. The updating is based on a hyperbolic moveout analysis on the inverted NMO-CIP gather obtained from PKTM, which is performed to produce a CIP gather using the initial stacking velocity model. The CIP gather is then inverted using the hyperbolic moveout with the initial velocity. A hyperbolic moveout analysis is applied to this inverted NMO-CIP gather to produce a velocity spectrum which can be used to update the velocity model.

Figure 7 shows an example of the migration velocity model and the corresponding CIP gather at the location CIP 350 of CIP line 050 from the data of shot line 5002 and receiver line 5002; these lines are collinear. Comparing Figures 7 and 6, we find that the events in Figure 7 are clearer and more focused than those in Figure 6. The velocity ratios γ_0 and γ_{eff} in the migration velocity model (Figure 7) are taken from the stacking velocity model (Figure 6) without any updating. As in Figure 6, anisotropy parameter χ is set to zero. Note that in both figures, the events in the CIP gather are flattened with the anisotropy parameter $\chi = 0$. This indicates that any VTI anisotropy in this data set is very small and can be neglected.

Azimuthal anisotropy. To examine the azimuthal anisotropy in the migration velocity model, we apply the updated migration velocity model at CIP line 050 to the data obtained from shot line 5018 and receiver line 5002. Shot line 5018 is 500 m from receiver line 5002. Figure 8 shows a CIP gather obtained using the updated velocity model at CIP 350 of CIP line 050. The raypath in this CIP gather is different from that for the CIP gather in Figure 7. The raypath for the CIP gather in Figure 7 has only one azimuth. However, the raypath for the CIP gather in Figure 8 has a wide range of azimuths. If azimuthal anisotropy is present, the migration velocity models for the two CIP gathers should be different. However, using the same updated migration velocity model, we can flatten the events in both CIP gathers. This means that, although the raypaths of PS-converted waves at this location from two shot lines are different, the velocity models are the same which, in turn, implies that the velocity model is azimuthally independent as well as spatially consistent.

We tested the migration velocity model at various locations for data from different shot and receiver lines. All results show that the azimuthal (HTI) anisotropy in this data set is small and can be neglected. This means that the migration velocity model in this area is isotropic and varies only with CIP location. Thus, only V_{PS}, γ_{eff}, and γ_0 need to be estimated from the data. Due to the azimuthal independence of the velocity model and the assumption of CIP-consistency, the velocity model at any CIP location can be estimated from single shot-line data. This saves a lot of processing time. Figures 9 and 10 show the profiles of V_{PS} and γ_{eff} at the location of CIP line 050. Once the migration velocity models at the CIP locations have been estimated, the 3D PKTM can be performed for all data sets using the updated velocity model.

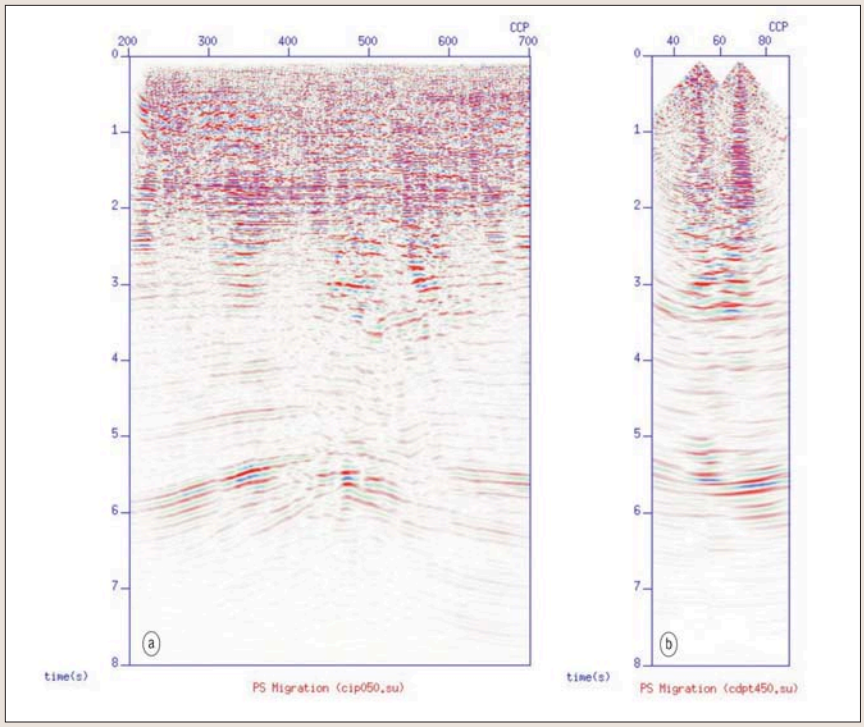

Figure 15. *(a) Inline projection at CIP line 050 and (b) crossline projection at CIP 500 from the 3D cube of the migrated image.*

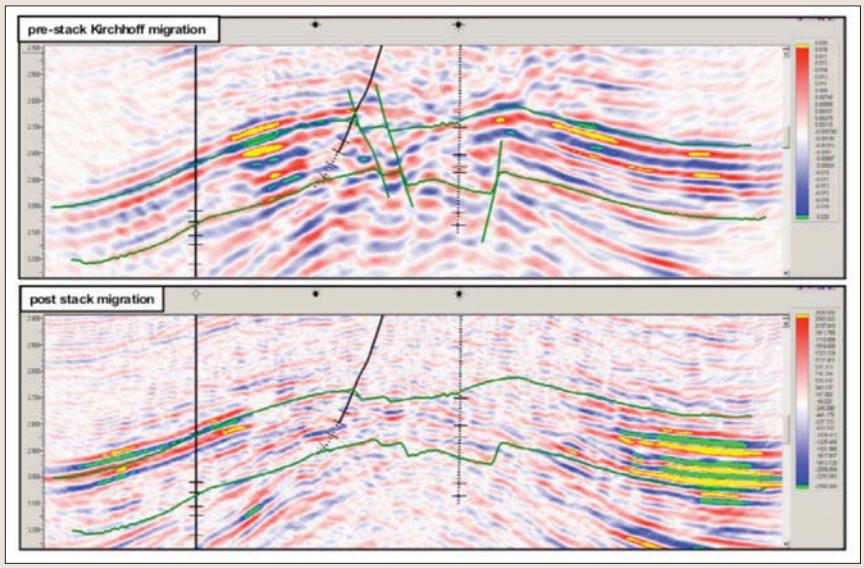

Figure 16. *A comparison between the PS-converted wave results (displayed in PP time) obtained using the PKTM approach (upper figure) and by conventional time processing (ACP, NMO, DMO stacking, postmigration) (lower figure). Drilling locations are marked on both images (black lines).*

Results of 2D processing. The data for 2D processing are from two shot lines. The locations of the shot lines are directly over the receiver cables (cables 5002 and 5018). They can therefore be treated as two 2D lines. 3D PKTM is reduced to 2D PKTM when the desired output line, source line, and receiver line are collinear. For one 2D line, we processed the P-wave data first. Figure 11 shows the stacked P-wave section and the migrated P-wave image at the location of receiver line 5002. In Figure 11, one can see that the image of the targets at about 3 s between CDP 400 and 600 has disappeared due to the gas clouds above them (between 1 and 2 s). Although the overall structure in the migrated image is clearer than that in the stacked section, the targets beneath the gas clouds still cannot be seen in the migrated image.

However, the image obtained from PS-converted waves displays the structure beneath the gas clouds. Figure 12 shows the stacked PS-converted wave section and the migrated PS-converted wave image in PP time at the location of receiver line 5002. The target beneath the gas clouds is faintly visible in the stacked PS-converted wave section (Figure 12a). It is more clearly seen in the migrated PS-converted wave image (Figure 12b). This is because, if the raypath of the downgoing P-wave is outside the gas cloud and the raypath of the upgoing converted S-wave is inside the gas cloud, we can observe the signal of the PS-converted wave at the receiver. The quality of the migrated PS-converted wave image is much better than the stacked PS-converted wave section and migrated P-wave image. The migrated PS-converted wave image at around 3 s in PP-time clearly shows the structure of interest with faulting at the dome beneath the gas cloud. The details of the faults in the target can be clearly identified in the migrated PS-converted wave image. However, these cannot be seen in the migrated P-wave image and stacked PS-converted wave section. This clearly shows the advantages of applying PKTM to PS-converted waves to image the structure beneath the gas cloud.

Results of 3D processing. 3D processing was applied to one swath of the data set, consisting of 22 shot lines. The signals from each shot line were recorded on two receiver cables. At one CIP line location, we can obtain a migrated image (subimage) from every shot line and one of two receiver cable lines. This migrated image contributes the final image at this CIP line location. The final image at each CIP line is the summation of 44 subimages obtained from 22 shot lines and two receiver lines. To produce these subimages, we performed 3D PKTM at the location of every CIP line for every pair of shot and receiver cable lines.

PKTM is computationally intensive. For example, it takes 16 hours to produce one subimage on a Sun workstation or a Linux PC. Because the final 3D image consists of 60 CIP lines, we would need 960 hours (40 days) to migrate one shot line data and 42 240 hours (1760 days) to migrate one suite of swath data. These timescales are not practical. To speed up this migration procedure, we perform the 3D PKTM on a PC cluster. The details of the parallel 3D PKTM on the PC cluster can be found in Dai (2005). Using 16 CPUs, we can produce one subimage in one hour. The total time for migrating data from one shot line data and one receiver line is 60 hours, and the total time for migrating one suite of swath data is 2640 hours (110 days). After data from all 22 shot lines and two receiver lines are processed, we sum the subimages of PS-converted waves at the locations of each

CIP line. The summed images form a 3D image cube of the PS-converted waves. Figures 13 and 14 show the 3D cube. Figure 15 shows the projections of the images at CIP lines 050 and CIP 500.

At the top of the cross-section, the upside down "w" shape is caused by the aperture control that applies the muting to the images. The migrated image has two peaks at the location of receiver lines 5002 and 5018, where the images have the strongest energies. The energy variation affects the image most at shallow depths (between 0 and 3 s in PS time). The difference in the curves can be clearly observed in the migrated images. This uneven distribution of energies at the locations between receiver lines may lead to the appearance of false structures in the images. Using more receiver lines may overcome this problem. The energy variation is smaller for the images in the deep part. Note that the consistency of images at times between 5 and 6 s shows that the structures are not related to the locations of the receiver lines. That means that this spacing of receiver lines is adequate to image deep structures.

Comparing the 3D migrated images with the 2D migrated images (Figures 12b and 15a), we find that although the targets in the 2D image and 3D image at the same locations have similar features, the details of the target are a little different. For example, at the location of CIP line 050, the target in both images at around 5.5 s in PS-time shows faulting at the dome beneath the gas cloud. However, the targets in the 3D image are smoother and more continuous than that in the 2D image, and the signal-to-noise ratio is higher in the 3D image than that in the 2D image. The same improvement in the 3D images can be found for other CIP lines.

Drilling results. The structure in the 3D migrated images has been confirmed by drilling at this area. Figure 16 shows one example of the comparison between the images obtained by our PKTM approach and by conventional PS-time processing (ACP, NMO, DMO, stacking, postmigration). Wells and interpreted horizons are marked on both images. In the image obtained from conventional processing (the lower plot in Figure 16), we cannot see faults. However, the PKTM result clearly shows the structure with dome faulting which is confirmed by drilling.

Conclusions. In this paper, we have developed a practical approach to performing 3D PKTM and applied this approach to processing PS-converted waves in a 3D/4-C data set from the North Sea. There are two key elements in this processing. One is to build the migration velocity model and the other is to perform the parallel 3D-PKTM in a PC cluster. Two steps are involved in building the velocity model—estimating the stacking velocity model and updating the velocity model for migration. The results obtained from both the stacking velocity model and migration velocity model show that neither VTI nor HTI anisotropy can be observed in this data set. An isotropic and CIP-consistent velocity model is therefore sufficient for image processing.

The processing results obtained from two 2D lines, where the shot line overlies the receiver cable line, show that PS-converted waves do have advantages over P-waves in imaging structures beneath gas clouds. To migrate the 3D data set, a scheme is specially designed to divide the whole job into subjobs that can independently perform 3D PKTM for a 2D line data. Each subjob is then performed by running a parallel version of the 3D PKTM on a PC cluster to speed up the migration processing. This 3D PKTM approach is efficient and robust. The processing results from 3D PKTM are encouraging and reveal the structure of the targets in greater detail. The structure beneath the gas clouds is clearly imaged using PS-converted waves with 3D PKTM. Faulting in the target area can be clearly identified in the migrated images. These structures have been confirmed by drilling.

Suggested reading. "Parallel processing of prestack Kirchhoff time migration on a Beowulf cluster" by Dai (*Computers and Geosciences*, 2005). "Integrative analysis of anisotropy parameter and velocities for PS converted waves" by Dai (*SEG 2003 Expanded Abstracts*). "Migration velocity analysis of PS-wave using INMO-CIP gathers of PKTM: A case study from the Gulf of Mexico" by Dai and Li (*EAGE 2003 Extended Abstracts*). "The effects of migration velocity errors on traveltime accuracy and the image of PS converted waves" by Dai and Li (GEOPHYSICS, 2006). "Anisotropy migration and model building for 4C seismic data: A case study from Alba" by Dai and Li (*SEG 2001 Expanded Abstracts*). "Imaging through gas-filled sediments using marine shear-wave data" by Granli et al. (GEOPHYSICS, 1999). "Seismic migration problems and solutions" by Grey et al. (GEOPHYSICS, 2001). "Converted-wave moveout and conversion-point equations in layers VTI media: theory and applications" by Li and Yuan (*Journal of Applied Geophysics*, 2003). "Converted-wave imaging of Valhall reservoir" by Thomsen et al. (*EAGE 1997 Extended Abstracts*). "Converted-wave reflection seismology over inhomogeneous, anisotropic media" by Thomsen (GEOPHYSICS, 1999). TLE

Acknowledgments: The authors thank Kerr-McGee North Sea (UK) Ltd., Talisman Energy, Total E&P UK Plc, and ExxonMobil for permission to show the data. This work is funded by the Edinburgh Anisotropy Project (EAP) of the British Geological Survey and is published with the permission of the executive director of British Geological Survey (NERC) and the EAP sponsors: BG, BGP, BP, Chevron, ConocoPhillips, CNPC, ENI-Agip, ExxonMobil, GX Technology, Kerr-McGee, Landmark, Marathon, Norsk Hydro, PDVSA, Shell, Schlumberger, Total, Veritas.

Corresponding author: hcd@bgs.ac.uk